

Investigation on the hydrodynamic scaling effect of an OWC type wave energy device using experiment and CFD simulation

Saishuai Dai*, Sandy Day, Zhiming Yuan, Haibin Wang

*University of Strathclyde, Naval Architecture, Ocean and Marine Engineering department,
Glasgow, United Kingdom*

Abstract

This paper presents a study of the effect of model scale on the performance of a fixed Oscillating Water Column (OWC) type Wave Energy Converter (WEC). Tank tests at two different scales, including the effect of scaling of the test tanks to minimise the bias introduced by different wave blockage effects. CFD simulations based on Reynolds Average Navier Stokes (RANS) method were then carried out for both scaled OWCs to investigate whether CFD simulation is able to reproduce the scale effect. Comparison between the tank test results and the CFD simulation results suggests that CFD simulation is capable of reproducing the hydrodynamic scaling effect with a good accuracy. Results also suggest that the hydrodynamic scaling effect is mainly introduced by the Reynolds number effect for cases investigated in the current study.

Keywords: Tank test, CFD simulation, Scale effect, Wave energy, Oscillating Water Column;

1. Introduction

Being one of the promising renewable energy technologies, WECs have attracted worldwide attention during the last few decades as one of the more promising marine renewable energy technologies. Detailed reviews of wave

*Corresponding author

Email address: saishuai.dai@strath.ac.uk (Saishuai Dai)

5 energy technologies can be found in several studies, for instance, [1],[2] and
6 [3]. Among all the proposed WEC technologies, the Oscillating Water Column
7 (OWC) type WEC is probably one of the most extensively studied technologies
8 due to its simple working principle [2].

9 Along with tank test, numerical studies of OWC type WECs have played an
10 important role in accelerating the evolution of OWC technology. For example,
11 Evans [4] derived the theoretical maximum efficiency for a 2D fixed symmetric
12 OWC device by assuming that the OWC surface moves as a weightless rigid
13 piston. Later Sarmento and Falcão [5] improved the theory by allowing OWC
14 surface variations using a surface pressure method and wave flume experiments
15 were carried out to validate the surface pressure theory [6]. With the help
16 of rapid development of computer technology, researchers started to simulate
17 the OWC problem with more advanced methods, such as BEM [7] and CFD
18 [8]. Different aspects of the OWC technology have been extensively studied by
19 several researchers, such as hydrodynamic performance [9], optimisation of the
20 OWC geometry [10] and optimisation of turbine-induced damping [11] etc.

21 Although significant progress on the development and understanding of the
22 OWC technology has been made recently, there are still several challenges to
23 overcome in performance prediction. The effect of model scale is probably one
24 of the critical issues in the early development stage, since the assessment of
25 the full-scale device performance is normally extrapolated from a model scale
26 experiment or simulation result at the early stage. To fill the gaps in theory
27 and guidelines for the requirements of scale testing of a WEC, Sheng et al. [12]
28 presented a theoretical analysis on the scaling of physical modelling and power
29 take-off system. In order to minimise viscous effects, it was recommended that
30 a physical model test shall be carried out with critical Reynolds number above
31 about 10^5 . This requirement, however, can not always be fulfilled especially for
32 tests in relatively small wave tanks since the scale (hence Reynolds number) of
33 the test is normally constrained by the tank size. In contrast, numerical simula-
34 tion methods such as CFD do not have the same limitations of scale. Recently,
35 Elhanafi et al. used an experiment-validated CFD model to investigate the air

compressibility effect at full scale [13]. Although those simulation works are validated against scaled tank test and excellent agreement between the simulation results and experiment results is achieved, there are, however, few published multi-scale tank test data which can validate the capability of simulation tools' to reproduce the aerodynamic and hydrodynamic scale effects.

Recently, Viviano et al. [14] tested a generalized small scale OWC and the results were compared with a similar large scale model to investigate the scale effect. In their study, OWC devices have the same width as the tank width. Therefore, 3D radiation and diffraction effect was excluded. This paper investigates two different scale tank tests of an idealized 3D OWC device. Corresponding CFD simulations are then performed to investigate whether CFD simulation is capable of capturing the hydrodynamic scale effect. This work is structured as below: Section 2 describes the experimental work including a discussion of the uncertainty and error source. Corresponding CFD simulations are described in Section 3. Section 4 compares the results obtained from the tank tests and CFD. Conclusion and future works are summarized in Section 5.

2. Physical experiments

Offshore structures (such as offshore platforms) are generally designed in such a way so that the interaction with waves is small. Guidance for these structures on wave blockage may therefore not be well-suited to WECs which are designed to have maximum wave structure interaction. Wave blockage in this context refers to all hydrodynamic effects related to the transverse constraints of the tank walls on the hydrodynamic response – including wave reflection from the tank walls and local variation in flow velocity caused by reduced cross section area due to the presence of the model. Therefore, the impact of wave blockage on results should be carefully considered [15], especially when comparing the performance of two different scale devices, since the effect of wall reflections and flow variations may be confused with the scale effect.

64 2.1. Facilities

65 In order to minimise the bias from different wave blockage introduced by
66 different tank widths, experiments were carried out in the Kelvin Hydrodynamic
67 laboratory and the Henry Dyer Hydrodynamic Laboratory of the University of
68 Strathclyde as shown in Figure 1. The Kelvin Hydrodynamic Laboratory has a
69 dimension of $76\text{ m} \times 4.6\text{ m} \times 2.5\text{ m}$ with water depth of 2.1 m and the Henry Dyer
70 Hydrodynamic Laboratory has a dimension of $21.6\text{ m} \times 1.53\text{ m} \times 1\text{ m}$ with water
71 depth set to 0.7 m. Since the cross section dimesion govern wave blockage, it is
72 anticipated that these two tanks will provide similar wave blockage effect when
73 the two models have a scale ratio of 3:1. Both tanks are equipped with flap
74 type wave makers and a wave absorbing beach. For convenience, Kelvin tank
75 is denoted as the large tank and Henry Dyer tank is denoted as the small tank
76 hereafter.

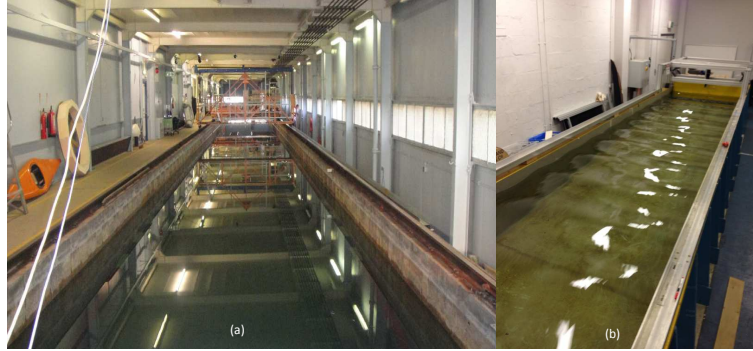


Figure 1: (a) Kelvin Hydrodynamic laboratory. (b) Henry Dyer Hydrodynamic laboratory.

77 2.2. OWC device

78 Simple acrylic hollow cylinders were selected to model an idealized OWC
79 device for further investigation. Such a simple geometry allows easy scaling
80 of the air compressibility by simply keeping the height of the air chamber the
81 same for both scales [12]. A smooth plastic ring collar was fitted to the bottom
82 of the device in order to have a better control of the sharp corners during the
83 geometry scaling process and at the same time. (see Figure 2 for detail.). The

84 Power Take Off (PTO) system was modelled using an orifice plate to simulate
 85 an idealised impulse turbine, because it has approximately quadratic pressure-
 86 flow rate characteristics. This method of modelling the PTO has been used by
 87 several researchers, for example, [13] and [16]). Instead of manufacturing several
 88 different size orifice plates, 8 equal size and equally spaced circular openings were
 89 drilled into the covering lid. By choosing different number of orifices open to
 90 the air, different levels of damping could be achieved. More detailed geometry
 91 information can be found in Table 1.

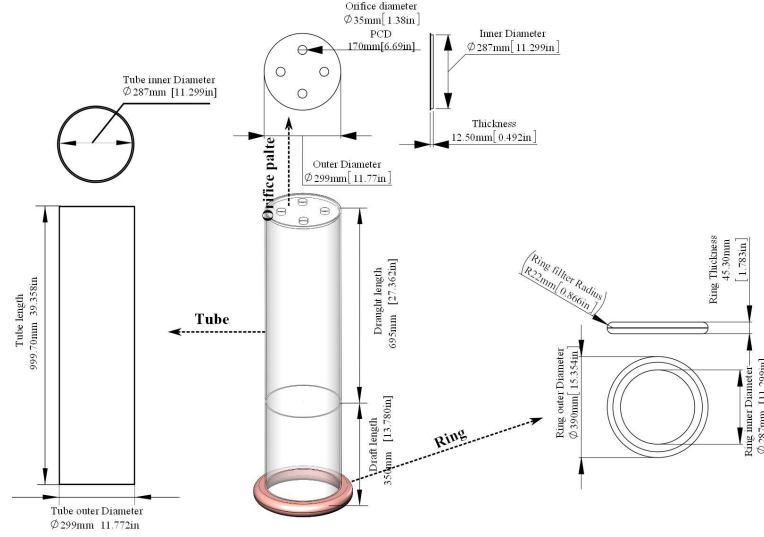


Figure 2: CAD illustration of the large scale device.

92 2.3. OWC performance and testing procedures

93 When assessing the performance of the OWC device, it is critical to assess
 94 the available wave power from the incident wave. Conventionally, a reference
 95 wave probe is located some distance in front of the device (i.e. between device
 96 and wave maker) to measure the incident wave. That measured incident wave
 97 information may be different from the wave arriving at the device due to spatial
 98 variations of waves in the tank and effects of wave decay. Besides, the wave
 99 measured by the reference probe may include the waves due to radiation (from

Table 1: Geometry details of the two OWC devices, scale ratio 1:3.

Component	Parameters (mm)	Large scale	Small scale
OWC model	total length	1045.0	808.5
	draft	350.0	116.7
Orifice plate	Plate Diameter	299.0	100.0
	Thickness	12.5	4.0
	Orifices Diameter	35.0	11.6
	Orifices position (PCD)	170	56.5
Tube	Outer Diameter	299.0	100.0
	Inner Diameter	287.0	96.0
Ring	Inner Diameter	299.5	100.5
	Outer Diameter	390.0	130
	Thickness	45.3	15.1
	Fillet radius	22.0	7.5

100 wave and OWC interaction) and scattering as well as the incident wave. There-
 101 fore, in the present work, taking the advantage of the high level of repeatability
 102 of the wave makers, the waves were first calibrated at the target location where
 103 the devices would be deployed prior to installation of the model. The incident
 104 average wave energy flux (P_{avail}) can then be determined by the calibrated wave
 105 information through

$$P_{avail} = \frac{1}{2} \rho g A^2 C_g \quad (1)$$

106
 107 where ρ is the density of water, g is the gravitational acceleration, A is the
 108 measured wave amplitude and C_g is the wave group velocity defined as

$$C_g = \frac{1}{2} \frac{\omega}{k} \left(1 + \frac{2kh}{\sinh(2kh)} \right) \quad (2)$$

109 The ω, k, h in Equation 2.3 are the circular wave frequency, the wave number
 110 and the water depth, respectively.

111 Devices were then fixed in the center-line of each tank. Regular waves with
 112 non-dimensional frequencies (Kh , here $K = \omega^2/g$) from 2 to 8 with constant
 113 wave height (0.06m for the large scale test and 0.02 for the small scale test.)
 114 were then tested. The mean captured power by the OWC device is calculated
 115 via

$$P = \frac{1}{T} \int_0^T \Delta p(t) q(t) dt \quad (3)$$

116 where T is the wave period and $\Delta p(t)$ is the instantaneous pressure difference
 117 across the orifice plate. This is measured by a differential pressure transducer
 118 installed on the top of the orifice plate. A Honeywell 163PC0D75 (± 622.27 Pa)
 119 low pressure differential transducer was used for the large scale tests and a SEN-
 120 SIRION SDP1000-L025 (± 62 Pa) low differential pressure sensor was employed
 121 to measure the pressure for the small scale tests, $q(t)$ in Equation 2.3 is the
 122 instantaneous volume flow rate driven by the water column and is defined by

$$q(t) = A_w \frac{\partial \eta}{\partial t} \quad (4)$$

123 where A_w is the cross section area of the OWC and η is the OWC elevation
 124 measured by wave probes located in the middle of each device.

125 To compare the performance of the two devices, the so called capture factor
 126 (capture width ratio) is introduced, defined as

$$Cf = \frac{P}{P_{avail} D_{out}} \quad (5)$$

127 where D_{out} is the characteristic length of the WEC device. In this case, D_{out}
 128 is the outer diameter of the OWC device (tube).

129 2.4. Experiment uncertainty and error

130 Uncertainty analysis was performed in line with International Towing Tank
 131 recommendation and guidelines ([17],[18]) in this paper. The main uncertainty
 132 source in the test comes from the instruments used for measurements. This kind
 133 of uncertainty (Type B, or systematic uncertainty) can be quantified through

instrument calibration or stated by the manufacturer. Combined with Type A (random uncertainty) obtained from repeated tests, uncertainty in the physical quantity of interested (e.g. mean captured power) can be calculated using uncertainty propagation analysis. For example, the total uncertainty in the peak mean power captured (1.1 W) caused by the pressure and volume flow rate measurement is 0.047 W for the large scale test. Detailed information on uncertainty analysis can be found in the above references. In the present study, the results of uncertainty analysis will be presented via error bars showing 95% confidence intervals with testing results.

Apart from the uncertainties whose impact can be directly assessed in the form of physical quantities of interest, there exist some uncertainties that cannot be modelled explicitly by uncertainty propagation. For example, the uncertainty in the draft will lead to an uncertainty in the natural frequency of the OWC and hence, in turn uncertainty in the captured power. These kind of uncertainties cannot be directly related to the final power output through uncertainty propagation rules, and therefore can only be quantified separately. The draft was set by visual alignment of the water surface and the draft line; hence the effect of the meniscus may lead to a draft different from the target value. The uncertainty in the draft is estimated to be about 1-2 mm . Similar uncertainties includes the uncertainty in the orifice size measurement, roundness of the OWC tube and the non-horizontality of the water column surface. Although no transversal oscillations were observed during the tests, it should be noted that the non-horizontality of the water column surface may bias the volume flow rate determination since the cross-section area in equation 4 is assumed to be flat and horizontal.

In addition to the uncertainties, there are also some known and unavoidable scaling discrepancies between the two models to available materials and manufacturing accuracy. For instance, the diameter of the tube and the thickness of the orifice plate are not scaled precisely, as shown by Table 1.

163 3. CFD simulation

164 To simulate the air-water two phase interaction problem, a Finite Volume
165 Method (FVM) based software STAR-CCM+ is selected to simulate the two
166 different scale OWC devices. This software has been widely used by several re-
167 searchers to simulate the OWC problem, for example Lopez[11] and Elhanafi[13].

168 3.1. Governing equations and numerical solver settings

169 Star-CMM+ uses a predictor-corrector method to link the continuity and
170 momentum equations. The shear stress transport(SST) $k - \omega$ model [19] is se-
171 lected in current work to model the turbulence. The Volume of Fluid (VOF)[20]
172 method along with high-resolution interface-capturing (HRIC) scheme [21] are
173 employed to resolve the free surface. Simulations are carried out by using a
174 segregated flow model and isothermal ideal gas is selected to account for the air
175 compressibility. The isothermal law is selected in current study because of the
176 fact that the air compressibility and temperature variation at such small scales
177 are negligible. Assuming isothermal avoids solving an ordinary energy transport
178 equation, and hence reduces computational time.

179 3.2. Numerical wave tank construction

180 Wave generation is realised by specifying the time varying wave particle
181 velocity and wave elevation (hence the phase volume fraction) at the inlet of
182 the CFD domain (Figure 3). Fifth order Stokes wave theory is adopted to
183 calculate the required velocity and wave elevation profile.

184 Wave damping at the end of the Numerical Wave Tank (NWT) is achieved
185 by introducing a resistance to the vertical motion in the form of a momentum
186 source in a pre-defined zone (for example, zone B in Figure 3) [22]. The length
187 of the damping zone B is set to be two wavelength (λ) for good absorption
188 performance.

189 Wave reflection from the inlet boundary is absorbed using the Euler Overlay
190 Method (EOM) [23]. This method computes the difference between the analyt-
191 ical wave information and the actual wave information in the specified region

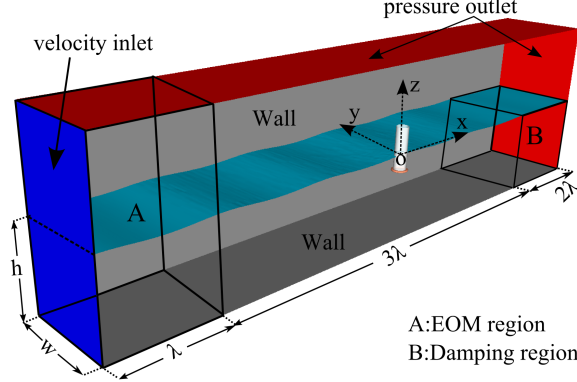


Figure 3: CFD domain and boundary conditions. Here h is the water depth (2.1 m for the large scale and 0.7m for the small scale.) and w is half tank width (2.3 m for the large scale and 0.765 m for the small scale simulation.)

192 (zone A in Figure 3, the actual wave is then forced to the analytical wave by
 193 adding corresponding source or sink into the governing equations. The source
 194 or sink term takes the following form

$$S(\phi) = -c(\phi - \phi^*) \quad (6)$$

195 Where $S(\phi)$ is the source or sink corresponding to variable ϕ (time varying wave
 196 particle velocity distribution along the water depth direction and instantaneous
 197 wave elevation .). In order to make a smooth transition between the computed
 198 and the analytical results, a distance dependent weighting function c is intro-
 199 duced into the source and sink term. The weighting function has the following
 200 form

$$c = c_0 \cos^2(\pi x/2) \quad (7)$$

201 Where c_0 is the maximum value of the forcing coefficient and x is the relative
 202 distance within the EOM zone (x equals to zero at the beginning and 1 at the
 203 velocity inlet, meaning the forcing takes no effect at the end of the EOM zone
 204 and gives the maximum impact at the velocity inlet.). The choice of the value
 205 of c_0 is problem dependent [24], a value of 100 was found to be sufficient and
 206 efficient for the present work.

207 When wave generation is considered, mesh topology normally has a signifi-
 208 cant impact on the quality of the simulated wave due to numerical dissipation.
 209 A denser mesh can normally reduce the numerical dissipation at the cost of
 210 longer computation time. The mesh distribution around the free surface was
 211 first investigated by performing simulations of a selected wave with different
 mesh settings. Those simulations were executed in a pseudo-2D manner which

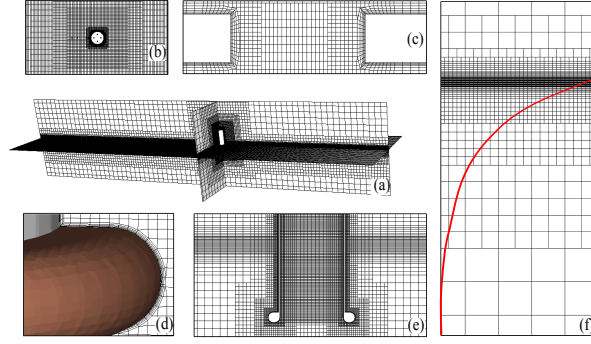


Figure 4: Mesh distribution: (a) overview of mesh distribution, (b) Mesh distribution at the free surface along tank width direction. (c) Mesh distribution around the orifice (sectional view). (d) Mesh distribution around the collar ring. (f) Free surface mesh distribution along water depth direction.

212
 213 employed only one cell in the tank width direction. The mesh distribution
 214 around the free surface was designed in such a way that the size of the mesh
 215 is controlled by the aspect ratio (defined as the ratio between the mesh size
 216 in the wave height and the wavelength direction.). The mesh topology in the
 217 water depth direction was decided based on the maximum water particle veloc-
 218 ity profile. For example, as shown in Figure 4 (f), the mesh gets coarser with
 219 increasing water depth as the water particle velocity (illustrated by the red solid
 220 line) reduces. Mesh aspect ratio of 1/2, 1/4, 1/8 and 1/16 were investigated.
 221 the resulting mesh resolution in the wave propagation direction varies from 60
 222 cells in one wavelength to 140 cells in one wave length with a uniform step of
 223 20 cells. The corresponding mesh resolution in the wave height direction is then
 224 decided by multiplying the mesh size in wavelength direction with the defined

225 aspect ratio. The total number of cells division within the wave height varies
 226 from about 5 to about 35 depending on the aspect ratio and the mesh resolution
 227 in the wavelength direction.

228 As for the numerical dissipation caused by the mesh, inappropriate temporal
 229 discretization will also lead to dramatic numerical dissipation. A second-order
 230 time discretization method is selected to resolve time marching for better accu-
 231 racy. Time step size Δt is decided based on the Courant-Fridrichs-Lewy (CFL)
 232 number via

$$\Delta t = \frac{CFL \cdot \Delta x}{u} \quad (8)$$

233 Where Δx is the size of a single cell at the free surface in x direction (see Figure 3
 234 for coordinate system). The denominator u is the wave phase velocity in current
 235 study. A CFL number of 0.5 is normally enough to meet the requirement of
 236 a second order temporal discretization scheme; in the present study a value of
 237 0.25 is selected to give an extra safe margin.

238 A regular wave with wave height equal to 0.06m at $Kh = 4.9$ is tested for
 239 those proposed mesh settings with correspondingly calculated time step size. It
 240 is found that a mesh aspect ratio of 1/8 provides the most economic result for
 241 the current study. Figure 5 demonstrates the spatial distribution of the wave
 242 elevation along the tank length after 40 seconds simulated physical time. As can
 243 be seen, the wave crest height increases with denser meshes in one wavelength
 244 indicating the numerical dissipation is relieved with denser mesh. Comparison of
 245 the wave height measured at 2 wavelength away from the wave generating inlet
 246 and the theoretical wave height suggests the maximum and minimum discrep-
 247 ancy is about 3.7% and 1.7%, respectively. With an improvement of only 2%,
 248 the simulation with 140 cells in the wavelength direction took about 17 hours
 249 on a desktop PC with 32G RAM and 4 core Intel I7-2600 processor (3.4 GHz)
 250 while the case with 60 cells only took about 2 hours with the same computer.
 251 The 80 cells simulation appears to be the most economic case with a discrepancy
 252 of about 2.9% and 3 hours running time. Therefore, this mesh setting for wave
 253 capturing is selected for the OWC simulations.

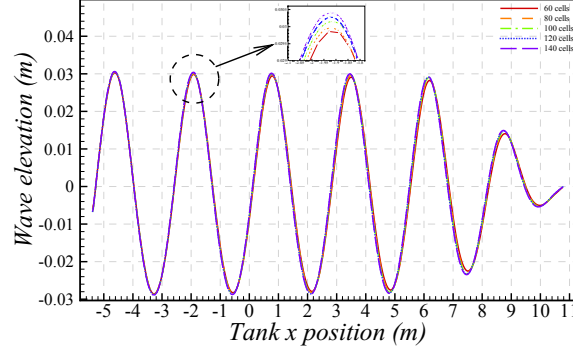


Figure 5: Mesh effect on the free surface elevation spatial distribution along the tank after 40 seconds simulated physical time. The legend states the number of cells in one wavelength.

254 Simulations using different time step sizes are executed to check the reliability of the proposed time step size determination method. The time step size
 255 calculated, based on Equation 2.3, yields about 0.004 seconds. As suggested by
 256 Figure6, simulation results converge when the time step size is smaller than 0.005
 257 indicating the validity of the proposed time step size determination method.

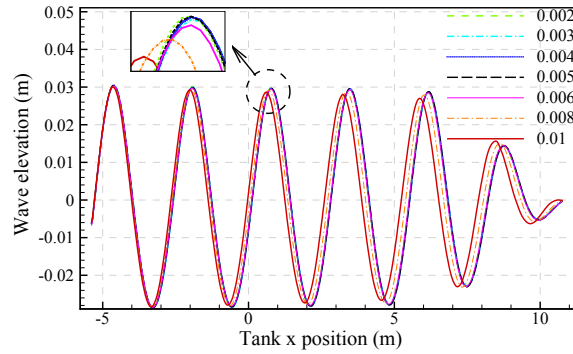


Figure 6: Time step size effect on the wave elevation after 40 seconds physical time simulation.

258

259 3.3. OWC simulation

260 The OWC device is then fixed in the middle of the NWT as shown in Figure
 261 3. Boundary conditions are illustrated in Figure 3. It should be noted here
 262 that simulations took advantage of the symmetry of the problem about the tank

263 centreline; hence, only half of the tank was simulated. The total length of the
 264 NWT is set to be 6λ which may or may not be sufficient for accurate simula-
 265 tion of the device's performance. This simplification is made due to the large
 266 demand of computational resource for the OWC simulations. The dense mesh
 267 inside the OWC device (Figure 4 (e)), the extra refined mesh around the orifice
 268 plate (Figure 4 (c)), the mesh refinement outside the OWC device at the free
 269 surface and the employment of modelling of the boundary layer at the device
 270 surface leads to a mesh with typically 2 million volume cells. The transients
 271 of the oscillation of the water column (especially at high frequencies) require
 272 long physical time to reach steady state. Along with the required small time
 273 step size, this places further demands on the computational resource required.
 274 A typical simulation (50 seconds simulated physical time) around the resonant
 275 point takes about 64 hours using 48 cores high performance computer (inter
 276 Xeon X5650 2.66 GHz CPU).

277 In the small scale simulation, the small scale OWC device was scaled directly
 278 from the large scale simulation according to proper scaling law, rather than
 279 reproduced according to the small scale device used in the small scale physical
 280 experiment. Hence, the CFD simulation does not have geometry scaling errors.
 281 In addition to waves, the mesh distribution and time step size settings for the
 282 small scale simulation are directly scaled according to Froude similarity rule as
 283 well.

284 **4. Results**

285 Study of the OWC device without orifice plate is first carried out to in-
 286 vestigate the scale effect on the hydrodynamics without PTO damping. These
 287 results are presented in section 4.1. Results of OWC with PTO damping are
 288 presented in Section 4.2.

289 *4.1. Tests with no PTO damping*

290 The Response Amplitude Operator, defined as the ratio between the mea-
 291 sured OWC motion amplitude and the incident wave amplitude are presented

in Figure 6 for both tank test and CFD simulations. The RAO obtained from the CFD simulation has been corrected assuming an incident wave amplitude reduction of 3% due to numerical dissipation based on the NWT study.

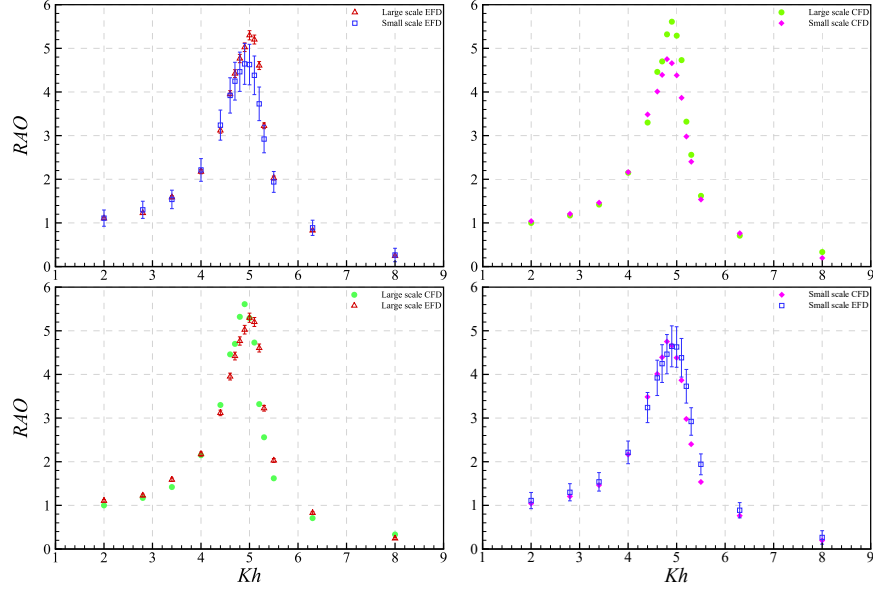


Figure 7: Comparison of RAO obtained from tank test(EFD) and CFD simulation for both large and small scales.

As suggested by Figure 7, the uncertainty in the small scale experiment is much higher than that of the large scale test. This large uncertainty comes from the uncertainty in the wave probes which were used to measure the OWC oscillation and incident wave. The absolute Type B (systematic) uncertainty introduced by those wave probes used in the small scale test is in fact similar to that of the large scale test. However, due to the scaled incident wave amplitude (and hence also the OWC response) the uncertainty in the RAO calculation increased dramatically through uncertainty propagation. In spite of the large uncertainty, it is clear that the response of the small scale test is smaller than that of the large scale test around the peak response frequencies even with such a large uncertainty. The comparison of the large and small scale CFD simulations

clearly confirmed this observation. The smaller RAO obtained from the small scale model can be explained by the dissimilarity of Reynolds number, that in the small scale OWC is much smaller meaning higher relative viscous losses.

The comparison of the CFD simulation and tank test result suggests the CFD slightly over predicts the peak RAO obtained from tank test for both scales. A frequency shift in the peak response frequency is also observed for both scales. The uncertainty in the draft in the tank test mentioned previously may contribute to the different in natural frequency. This difference in the natural frequency will in turn contribute to the difference in the peak response. Nevertheless, the difference in the peak response period is small. Table 2 lists the peak response period for CFD simulation and tank test.

Table 2: Peak response period obtained by CFD and tank test

	Large scale	Small scale
CFD	1.313 (s)	0.758 (s)
EFD	1.300 (s)	0.751 (s)

The maximum and minimum possible peak RAO based on the 95% uncertainty values for the large and the small scale tests are listed in Table 3. The corresponding possible maximum and minimum difference in the peak RAO between the large scale and the small scale tests are 1.23 and 0.08, respectively. The possible relative difference thus varies from 1.5% to 22.7% (the minimum relative difference is defined as the ratio of the minimum difference to the large scale minimum possible RAO value, and the maximum relative difference is defined as the ratio of the maximum difference to the large scale maximum possible RAO value.). Calculations based on the measured peak RAO suggest that the small scale test under-predicts the large scale by about 12.4%. Results from the CFD simulation suggest an absolute difference in the peak RAO of 0.86 yielding a relative difference about 15.3%.

Table 3: Tank test peak RAO and possible minimum and maximum value for the large and small scale OWC.

	Mearsured peak RAO	Uncertainty at peak RAO	Maximum possible RAO	Minimum possible RAO
Large scale	5.300	0.105	5.405	5.195
Small scale	4.644	0.469	5.113	4.175

4.2. Tests with PTO damping

Results are presented here for the case with 4 orifices open to the atmosphere. This configuration gave the maximum power output compared with other conditions (e.g. 8 orifices open to the atmosphere.).

The RAO, the pressure amplitude and the capture factor for OWC devices with modelled PTO damping are presented in Figure 8, Figure 9 and Figure 10, respectively.

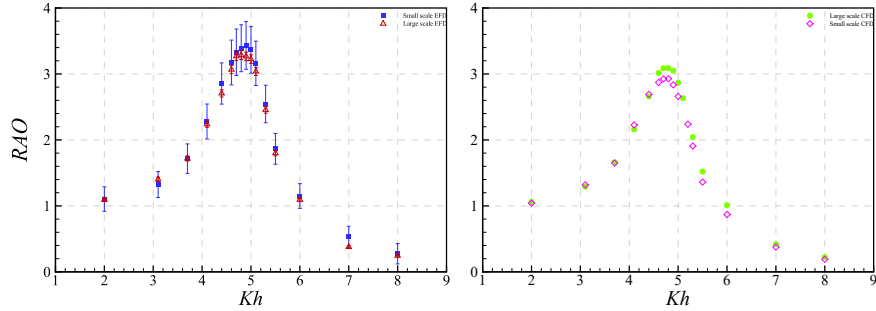


Figure 8: Comparison of RAO obtained from tank test(EFD) and CFD simulation for both large and small scales. PTO damping is set to 4 orifices open to the air.

The RAO of the small scale tank test suggests a larger response around the peak response frequencies compared with the large scale tank test, however, the large uncertainty covers the large scale results which makes the comparison less reliable. On the other hand, the CFD simulation suggests that the response of the small scale OWC is smaller than that of the large scale OWC.

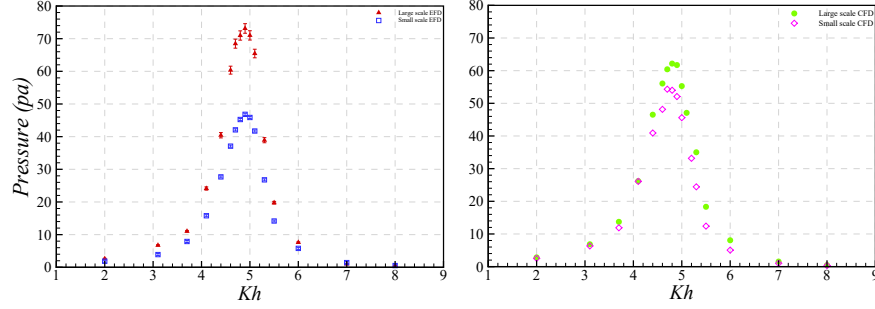


Figure 9: Comparison of pressure amplitude obtained from tank test(EFD) and CFD simulation for both large and small scales. PTO damping is set to 4 orifices open to the air.

341 The pressure amplitude obtained by the tank test and the CFD simulation
342 both suggest the small scale OWC has a smaller pressure amplitude around the
343 peak response frequency. According to the Froude scaling rule, the pressure
344 amplitude should scale with the geometric scale factor. It can be deduced from
345 Figure 9 that the small scale pressure amplitude is smaller than the pressure
346 amplitude of the large scale after extrapolation to the large scale. Comparing
347 the results between the tank test and the CFD simulation, it can be seen that
348 the peak pressure amplitude of the large scale simulation is smaller than that
349 of the tank test while the small scale simulation has a higher peak pressure
350 amplitude. The smaller pressure amplitude of the large scale simulation can be
351 explained by the NWT dissipation, which results in, the wave amplitude arriving
352 at the OWC device with smaller than the specified wave amplitude. The larger
353 pressure amplitude of the small scale CFD simulation will be explained in section
354 4.3.

355 Both the tank test and the CFD simulation suggest that the small scale
356 capture factor is smaller than that of the large scale. Table 4 lists the measured
357 maximum and minimum possible capture factor for the large and the small
358 scale tank test. Based on the maximum and minimum possible value, the small
359 scale test results under predict the large scale capture factor by about 24.5%
360 to 37.6%. The calculation based on the measured value suggests that the small

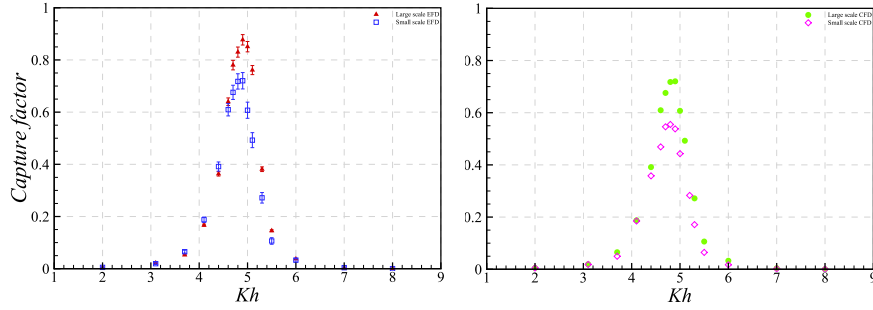


Figure 10: Comparison of capture factor obtained from tank test(EFD) and CFD simulation for both large and small scales. PTO damping is set to 4 orifices open to the air.

scale under predicts the large scale result by about 31%. On the other hand, the
CFD simulation results indicate that the small scale simulation under predicts
the large scale simulation by about 22.9%.

Table 4: Tank test peak capture factor and possible minimum and maximum value for the large and small scale OWC.

	Mearsured peak Cf	Uncertainty at peak Cf	Maximum possible Cf	Minimum possible Cf
Large scale	0.877	0.039	0.916	0.839
Small scale	0.602	0.031	0.633	0.571

4.3. PTO scaling

The modelled PTO system: the orifice plate, as mentioned previously, has
a quadratic pressure-flow rate characteristic as shown by Figure 11 and can be
described by

$$p = \Lambda q^2 \quad (9)$$

the damping coefficient Λ is a real number describing the relationship be-
tween the pressure and the volume flow rate.

As indicated by Figure 11, apart from the small scale tank test, all the other
pressure and volume flow rate amplitude relationship are very close to each

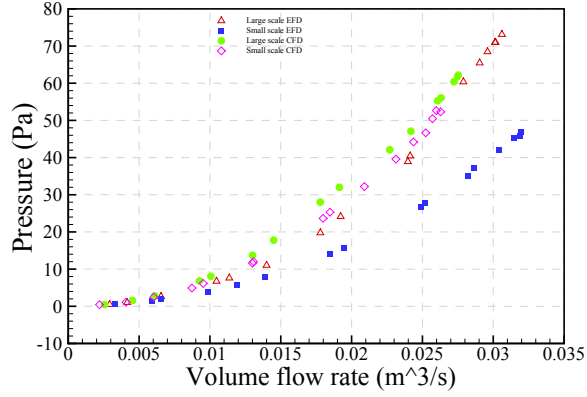


Figure 11: Pressure amplitude and volume flow rate amplitude relationship, here the small scale result are extrapolated to the large scale according to the Froude scaling rule. Each data point corresponding to a single frequency simulation/tank test.

other. This suggests that the damping applied in the small scale tank test is different from the damping used in the CFD simulation.

Following the Froude scaling rule, Λ should scale with s^{-4} , yielding 1/81 in the present work, here s is the scale factor defined as the ratio between the geometry dimension of the large scale and the geometry dimension of the small scale. The scale factor is 3 in the present study. Figure 12 compared the damping ratio (defined as $\Lambda_{small}/\Lambda_{large}$) for the tank test and the CFD simulation. This explains why the small scale CFD simulation has a larger pressure amplitude than the small scale tank test.

It is clear that the damping ratio of the tank test is far from the Froude-scaled value. This is because the small scale PTO was not scaled correctly due to the errors and uncertainties. The uncertainty in the damping ratio for the tank test is enormous due to the large uncertainty in the small scale OWC elevation measurement. On the other hand, the damping ratio of the CFD simulation is close to the theory ratio compared with the tank test result. However, it is still smaller than the theoretical value.

Figure 13 illustrates the relationship between the damping coefficient Λ and the orifice Reynolds number for the large and small scale CFD simulation. The

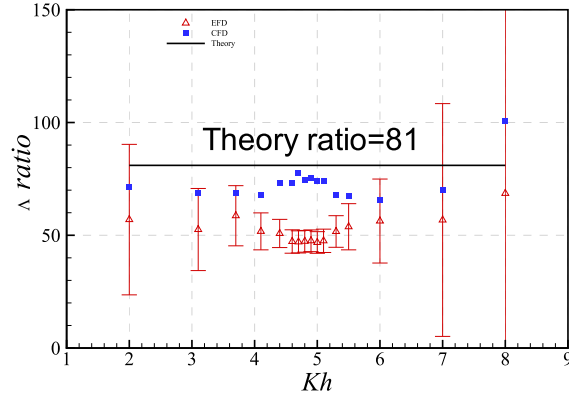


Figure 12: Comparison of the Λ ratio between the tank test and the CFD simulation.

orifice Reynolds number is defined as

$$Re = \frac{D \cdot U}{\nu_{air}} \quad (10)$$

where D is the characteristic length of the orifice plate and is defined as 2 times the orifice diameter (This characteristic length is decided to be the diameter of an orifice whose area is equivalent to the total area of the four orifice), U is the mean air velocity through the orifices, calculated by dividing the OWC volume flow rate by the total orifice area and ν is the dynamic viscosity of air.

Figure 13 suggests that for the large scale, the damping coefficient Λ is smaller at low Reynolds number and increases with increasing Reynolds number. With further increased Reynolds number (up to about $6.5E5$), Λ is found to reduce to some extent and tends to stabilize. The small scale simulation has a much smaller Reynolds number and it seems like that the extrapolated small scale Λ falls into the low Reynolds number region of the large scale Λ , suggesting the small scale Λ experienced Reynolds number effect.

4.4. CFD simulation of a larger scale OWC

Keeping the air chamber of the OWC device the same height as previous two scale simulations, a further extrapolation of three times larger than the large scale simulation is carried out. Figure 14 shows the comparison of the mean

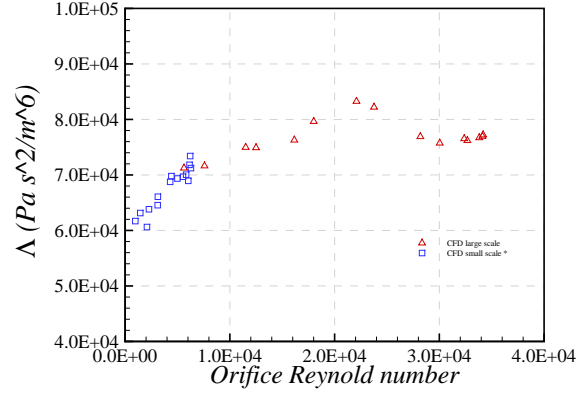


Figure 13: Reynolds effect on the Λ . Here the Λ of the small scale simulation is extrapolated to the full scale according to the Froude scaling rule while the Reynolds number is kept at small scale.

407 captured power for the three different scales and Table 5 summarises the results
 408 and relative differences.

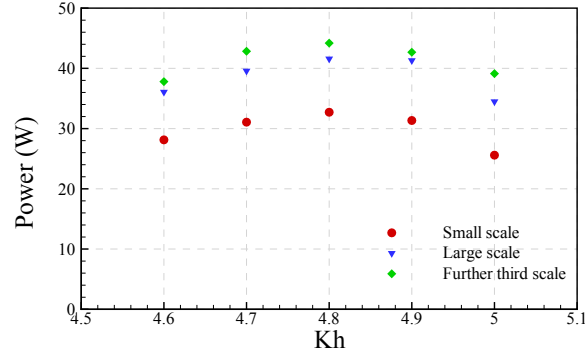


Figure 14: Comparison of the mean captured power for different scales. Power of the small scale and the large scale are extrapolated to the further third scale according to Froude scaling rule.

409 The large scale simulation under-predicts the values obtained for the further
 410 three-times scale by an average of 7% and the small scale simulation under-
 411 predicts the further third scale by an average of 28%. Figure 15 plots the peak
 412 mean power captured against the Reynolds number. Here the Reynolds number

Table 5: Mean power captured for the three different scales. Here the large scale and small scale power are extrapolated to the further 3 times larger scale using Froude scaling rule. The relative difference are calculated based on the further 3 times larger scale.

Kh	4.6	4.7	4.8	4.9	5.0
Further 3 times larger scale (W)	37.80	42.84	44.19	42.68	39.13
large scale (W)	36.06	39.57	41.58	41.31	34.48
small scale (W)	28.13	31.07	32.72	31.35	25.59
Relative difference (large scale)	-5%	-8%	-6%	-3%	-12%
Relative difference (small scale)	-26%	-27%	-26%	-27%	-35%

413 is defined according to [12] as

$$Re = \frac{A\omega D_{out}}{\nu_{water}} \quad (11)$$

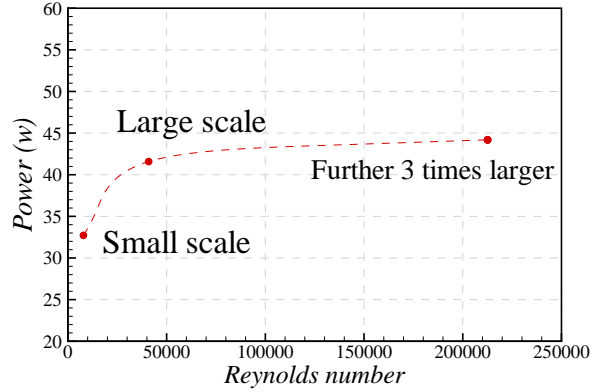


Figure 15: Peak mean captured power against Reynolds number.

414 As indicated by the trend line (dashed line) and Table 5, the small scale
 415 simulation experienced significant Reynolds number effect. On the other hand,
 416 the large scale simulation results were less affected by the Reynolds number.
 417 Judging by the trend line, it seems like Sheng's [12] recommendation of the
 418 critical Reynolds number (of the order of 10^5) is a good estimation.

419 5. Discussion and conclusion

420 This paper presents tank test and CFD simulation of two different scale
421 OWC type WEC. A CFD simulation three times larger again is presented for
422 further investigation of the scale effect.

423 The comparison between the tank test and CFD simulation of the cases
424 without the modelled PTO suggest that, in spite of the uncertainty in the draft
425 of tank test, the CFD simulation can predict the scale effect quite accurately.
426 The small scale CFD simulation under-predicts the large scale peak RAO by
427 about 15.3% while the tank tank test suggests a 12.4% difference.

428 When the modelled PTO is considered, very precise scaling of the orifice
429 at such scales is difficult for tank test. The damping provided by the orifice is
430 extremely sensitive to the size of the orifice at the small scale tank test. With
431 only 0.07 mm difference in the orifice diameter (hence 0.28 mm difference in
432 total since 4 orifices are used.) and 0.167 mm difference in the orifice plate
433 thickness, the volume flow rate and pressure relationship changed significantly
434 as suggested by Figure 11. In contrast, the CFD simulation is not restricted
435 by these practical scaling issues. The small scale CFD simulation provides a
436 similar volume flow rate and pressure relationship as the large scale simulation.
437 The CFD results indicate that the small scale simulation underestimated the
438 large scale peak capture factor by about 22.9% while the tank test suggests the
439 small scale tank test under-predicts the large scale by between 24.5% to 37.5%
440 considering the uncertainty. The relative difference between the small scale tank
441 test and the large scale tank test without considering the uncertainty is about
442 31%. The difference between the large scale and the small scale tank test is
443 anticipated to be smaller than 31% if the orifice of the small scale tank test
444 were able to be perfectly scaled.

445 The discrepancy between the large scale tank test of the OWC with PTO and
446 the CFD simulation is mainly due to the dissipation introduced by the NWT.
447 CFD simulations have uncertainties introduced by the mesh, the choice of time
448 step etc. A careful study of mesh and time step size impact should be carried

449 out to examine the errors and uncertainties for accurate simulation of the OWC
450 device. However, in this study, same numerical settings and mesh strategies
451 are adopted for all those different scales, it is assumed to be reasonable to
452 assume that the errors and uncertainties introduced are unidirectional and have
453 similar relative effect on the final output. Therefore, it will probably not affect
454 the comparison between different scales significantly. In order to accurately
455 simulate the performance of a WEC, it is suggested to calibrate the NWT in
456 advance and adjust the input wave in such a way so that the wave arriving at
457 the device is equal to the required value.

458 The performance of the modelled PTO system (the orifice plate) is affected
459 by the orifice Reynolds number as indicated by Figure 13. The orifice Reynolds
460 number is dependent on the motion of the OWC which is not known in ad-
461 vance. Therefore, it is recommended to check the Reynolds number effect on
462 the damping coefficient Λ afterwards to check whether the performance of the
463 orifice is strongly affected by the Reynolds number. If so, the orifice Reynolds
464 number should be reported along with the final result.

465 A further three-times scaled up CFD simulation result indicates that the
466 large scale simulation used here is not affected by the Reynolds number signifi-
467 cantly. Judging by the trend line (Figure 15), Sheng's [12] recommendation of
468 critical Reynolds number seems to be a good choice. It should be noted here
469 that for the further three-times scaled CFD simulation, the results may be more
470 affected by the air compressibility which would need further investigation. For
471 example, perform CFD simulation with a more realistic compressible air model
472 such as real gas model.

473 CFD simulations of the three different scale OWC in current study required
474 similar amount of computation resource since mesh and numerical settings were
475 scaled accordingly. On the other hand, the cost of the tank test increased with
476 the scale (mainly introduced by the cost of the facilities and model.). However,
477 the cost of the small scale tank test is in fact lower than that of the small scale
478 CFD simulations. It is still not cost-effective to investigate an OWC type WEC
479 at small scale (about 1:100 scale of a full scale device) using CFD simulation at

480 current stage.

481 **6. Future work**

482 Although the effect of side wall reflection is not reported in this work, pri-
483 mary tank test results indicate that a model breadth to the tank width ratio
484 of 0.2 is not enough to ignore the tank width effect for current OWC device.
485 Detailed work on the tank width effect will be reported in the future.

486 **Acknowledgement**

487 The CFD simulation results were obtained using the EPSRC funded ARCHIE-
488 WeST High Performance Computer (www.archie-west.ac.uk). EPSRC Grant
489 no. EP/K000586/1.

490 Authors would like to thank all reviewers for their valuable time and valuable
491 comments.

492 **References**

- 493 [1] J. Cruz, Ocean wave energy: current status and future perspectives,
494 Springer, Berlin. Science & Business Media, 2007.
- 495 [2] A. F. d. O. Falcão, Wave energy utilization: A review of the technologies,
496 Renewable and Sustainable Energy Reviews 14 (3) (2010) 899–918. doi:
497 <https://doi.org/10.1016/j.rser.2009.11.003>.
- 498 [3] N. Khan, A. Kalair, N. Abas, A. Haider, Review of ocean tidal, wave
499 and thermal energy technologies, Renewable and Sustainable Energy Re-
500 views 72 (2017) 590–604. doi:[https://doi.org/10.1016/j.rser.2017.](https://doi.org/10.1016/j.rser.2017.01.079)
501 01.079.
- 502 [4] D. Evans, A theory for wave-power absorption by oscillating bodies, Journal
503 of Fluid Mechanics 77 (1) (1976) 1–25.

- [5] A. J. Sarmento, A. d. O. Falcão, Wave generation by an oscillating surface-pressure and its application in wave-energy extraction, *Journal of Fluid Mechanics* 150 (1985) 467–485.
- [6] A. Sarmento, Wave flume experiments on two-dimensional oscillating water column wave energy devices, *Experiments in fluids* 12 (4-5) (1992) 286–292.
- [7] Y. M. C. Delauré, A. Lewis, 3d hydrodynamic modelling of fixed oscillating water column wave power plant by a boundary element methods, *Ocean Engineering* 30 (3) (2003) 309–330. doi:[https://doi.org/10.1016/S0029-8018\(02\)00032-X](https://doi.org/10.1016/S0029-8018(02)00032-X).
- [8] Y. Zhang, Q.-P. Zou, D. Greaves, Air–water two-phase flow modelling of hydrodynamic performance of an oscillating water column device, *Renewable Energy* 41 (2012) 159–170. doi:<https://doi.org/10.1016/j.renene.2011.10.011>.
- [9] A. Kamath, H. Bihs, i. A. Arntsen, Numerical investigations of the hydrodynamics of an oscillating water column device, *Ocean Engineering* 102 (2015) 40–50. doi:<https://doi.org/10.1016/j.oceaneng.2015.04.043>.
- [10] F. Mahnamfar, A. Altunkaynak, Comparison of numerical and experimental analyses for optimizing the geometry of owc systems, *Ocean Engineering* 130 (2017) 10–24. doi:<https://doi.org/10.1016/j.oceaneng.2016.11.054>.
- [11] I. López, B. Pereiras, F. Castro, G. Iglesias, Optimisation of turbine-induced damping for an owc wave energy converter using a rans–vof numerical model, *Applied Energy* 127 (2014) 105–114. doi:<https://doi.org/10.1016/j.apenergy.2014.04.020>.
- [12] W. Sheng, R. Alcorn, T. Lewis, Physical modelling of wave energy converters, *Ocean Engineering* 84 (2014) 29–36. doi:<https://doi.org/10.1016/j.oceaneng.2014.03.019>.

- [13] A. Elhanafi, G. Macfarlane, A. Fleming, Z. Leong, Scaling and air compressibility effects on a three-dimensional offshore stationary owc wave energy converter, *Applied Energy* 189 (2017) 1–20. doi:<https://doi.org/10.1016/j.apenergy.2016.11.095>.
- [14] A. Viviano, S. Naty, E. Foti, Scale effects in physical modelling of a generalized owc, *Ocean Engineering* 162 (2018) 248–258.
- [15] A. H. Day, A. Babarit, A. Fontaine, Y. P. He, M. Kraskowski, M. Murai, I. Penesis, F. Salvatore, H. K. Shin, Hydrodynamic modelling of marine renewable energy devices: A state of the art review, *Ocean Engineering* 108 (2015) 46–69. doi:<https://doi.org/10.1016/j.oceaneng.2015.05.036>.
- [16] D.-Z. Ning, R.-Q. Wang, Q.-P. Zou, B. Teng, An experimental investigation of hydrodynamics of a fixed owc wave energy converter, *Applied Energy* 168 (2016) 636–648. doi:<https://doi.org/10.1016/j.apenergy.2016.01.107>.
- [17] ITTC, Procedures and guidelines: Guide to the expression of uncertainty in experimental hydrodynamics, Report (2008).
- [18] ITTC, Recommended procedures and guidelines: Uncertainty analysis instrument calibration, Report 7.5-01-03-01 (2008).
- [19] F. R. Menter, Improved two-equation k-omega turbulence models for aerodynamic flows, NASA STI/Recon Technical Report N 93 (1992) 22809.
- [20] C. W. Hirt, B. D. Nichols, Volume of fluid (vof) method for the dynamics of free boundaries, *Journal of computational physics* 39 (1) (1981) 201–225.
- [21] T. Waławczyk, T. Koronowicz, Comparison of cicsam and hric high-resolution schemes for interface capturing, *Journal of theoretical and applied mechanics* 46 (2) (2008) 325–345.

- 558 [22] J. Choi, S. B. Yoon, Numerical simulations using momentum source
559 wave-maker applied to rans equation model, Coastal Engineering 56 (10)
560 (2009) 1043 – 1060. doi:[https://doi.org/10.1016/j.coastaleng.](https://doi.org/10.1016/j.coastaleng.2009.06.009)
561 2009.06.009.
562 URL [http://www.sciencedirect.com/science/article/pii/](http://www.sciencedirect.com/science/article/pii/S0378383909000970)
563 S0378383909000970
- 564 [23] J. Kim, J. O’Sullivan, A. Read, Ringing analysis of a vertical cylinder by
565 euler overlay method, in: ASME 2012 31st International Conference on
566 Ocean, Offshore and Arctic Engineering, American Society of Mechanical
567 Engineers, 2012, pp. 855–866.
- 568 [24] S. Enger, M. Perić, H. Monteiro, Coupling of 3d numerical solution method
569 based on navier-stokes equations with solutions based on simpler theories
570 (2014).